

Axion dark matter searches from the standard halo over the tidal stream to the big flow

Andrew K. Yi^a and Byeong Rok Ko^{b,1}

^a*SLAC National Accelerator Laboratory, 2575 Sand Hill Rd., Menlo Park, California 94025, USA*

^b*Department of Accelerator Science, Korea University Sejong Campus, Sejong 30019, Republic of Korea*

E-mail: andrewyi@slac.stanford.edu, brko@korea.ac.kr

ABSTRACT: The sensitivity of axion dark matter searches depends on the signal window that results from the velocity dispersion of axion dark matter. Since the ratio of signal windows is about 6500 between the standard halo and the big flow axion dark matter, each axion dark matter search usually uses a separate data acquisition (DAQ) channel with a different frequency resolution bandwidth (RBW). In this work, we demonstrate axion dark matter searches covering the standard halo, the tidal stream, and the big flow employing a DAQ channel starting with a single high resolution RBW, without sacrificing the DAQ efficiency, where the DAQ process includes online fast Fourier transforms and writing the outputs to disk. Assuming the total amount of data is sensitive to Dine-Fischler-Srednicki-Zhitnitskii (DFSZ) axion dark matter that follows the standard halo model and makes up 100% of the local dark matter density, the same data can also be used for the tidal stream and the big flow axion dark matter searches that would be sensitive to DFSZ axion dark matter that constitute 19.2% and 12.4% of the local dark matter densities, respectively, at a 90% confidence level. We also report that the filtering of the individual power spectra acquired with a relatively high resolution RBW e.g., for the big flow search can prevent a possible significant degradation in the signal to noise ratio from the searches in the lower resolution RBW's, i.e., the standard halo and tidal stream searches.

KEYWORDS: Dark Matter, Axions and ALPs, Beyond Standard Model

¹Corresponding author.

Contents

1	Introduction	1
2	Parameters	3
3	DAQ efficiency	3
4	Axion dark matter searches	6
4.1	Standard halo	8
4.2	Tidal stream	10
4.3	Big flow	11
5	Summary	12

1 Introduction

Cold dark matter (CDM) is believed to constitute about 85% of the total matter in our Universe from the standard model of Big Bang cosmology and high precision cosmological measurements [1]. The Standard Model of particle physics (SM) cannot explain CDM and the characteristics of CDM are still veiled to date even though there is strong evidence of its existence [2, 3]. One of the strong potential CDM candidates is the axion [4, 5] which was originally invented as a natural solution of the strong CP problem in the SM [6–10] and results from a breakdown of a new symmetry proposed by Peccei and Quinn [11]. Considering the current galaxy formation, dark matter has to be cold as aforementioned, or equivalently, non-relativistic, massive, and stable, which all fit the characteristics of the axion. Hence, axions are strong candidate which can be called “axion dark matter.”

The axion haloscope search which utilizes axion-photon coupling and a microwave resonant cavity proposed by Sikivie is the most sensitive axion detection method in the microwave region as of today thanks to the resonant conversion of axions to photons [12, 13]. Recent axion haloscope search experiments realized the Dine-Fischler-Srednicki-Zhitnitskii (DFSZ) axion [14, 15] sensitivity [16–20], assuming axions make up 100% of the local dark matter density ρ_a , i.e., $\rho_a = 0.45 \text{ GeV/cm}^3$,¹ and axion dark matter follows the standard halo model (SHM) [23]. The DFSZ axion can be implemented in grand unified theories (GUT) [24], thus supporting GUT as well as providing us with the understanding of the total matter in our Universe if DFSZ cold axion dark matter turns out to be responsible for 100% of the local dark matter density.

¹The axion community tends to use 0.45 GeV/cm^3 as a convention that was established long before, and in order to compare the sensitivity among different experiments it has remained that way. As dark matter density is a scalable variable to reach results, it is possible to convert our results here for given dark matter densities [21, 22].

In addition to the standard halo dark matter, dark matter streams complementary to the standard halo dark matter would contribute to the local dark matter density in their presence [25–27]. Two well-known dark matter streams that have distinct velocities v ’s and velocity dispersion δv ’s are dark matter of a tidal stream from the Sagittarius dwarf galaxy [25, 26] and that of the “big flow” [27]. Although our work here assumes the big flow exists based on ref. [27], we also point out that several studies [28–30] are skeptical of the feature proposed in ref. [27]. The contention regarding the astrophysical existence of the big flow itself is beyond this work’s scope, as it is more focused on optimizing the signal to noise ratio (SNR) across different possible axion dark matter models of varying bandwidths should they exist. Advancements in various aspects of the haloscope experiment will lead to better sensitivity, and this applies to all axion dark matter models. Expected SNR values in this work reflect the current reach of limits for an axion haloscope capable of searching for DFSZ axion dark matter for the SHM.

The tidal stream would have a $v \simeq 300$ km/s and a $\delta v \simeq 20$ km/s, while the big flow a $v \simeq 480$ km/s and a $\delta v \lesssim 53$ m/s, respectively. For dark matter whose mass is around 1 GHz, such v ’s and δv ’s result in the signal windows of about 150 Hz for the tidal stream and 0.625 Hz for the big flow, respectively, which are much narrower than that of the SHM dark matter of about 4 kHz. Because of such big differences in the signal windows, e.g., ~ 6500 between the SHM and the big flow, the required frequency resolution bandwidth (RBW) Δf of data for each axion dark matter search is also quite different, which can be handled with separated data acquisition (DAQ) channels with relevant RBW’s [31–34]. The difference between the SHM and the tidal stream is relatively smaller, thus one can perform both the SHM and the tidal stream axion dark matter searches using a DAQ channel with a single appropriate RBW as done in refs. [19, 35]. On the other hand, the recent interferometer based experiment also showed a feasibility that can do virialized and non-virialized axion searches in parallel [36].

In this work, we demonstrate axion dark matter searches covering the SHM, the tidal stream, and the big flow employing a DAQ channel with only one high resolution (HR) RBW, without sacrificing the DAQ efficiency ϵ_{DAQ} . Here the DAQ process includes online fast Fourier transforms (FFTs) and writing the outputs to disk. Using the data sensitive to the standard halo DFSZ axion dark matter with $\rho_a = 0.45$ GeV/cm³, the tidal stream and the big flow axion dark matter searches would be sensitive to DFSZ axion dark matter that constitute 19.2% and 12.4% of the local dark matter densities, respectively, at a 90% confidence level (CL). We also report that the filtering of the individual power spectra acquired with an HR RBW e.g., for the big flow search can prevent a possible significant degradation in SNR from the searches in the lower resolution RBW’s, i.e., the standard halo and tidal stream searches. We are referring to the filtering for the big flow searches [31–34] as “HR-RBW-filtering” in this work, where the HR RBW was chosen to be 0.025 Hz as explained in section 2.

2 Parameters

We used the parameters in ref. [19]. Particular parameters relevant to this work are listed in table 1. The 13 power spectra with $\Delta f = 0.025$ Hz correspond to 5200 power spectra with $\Delta f = 10$ Hz, and thus the expected sensitivity in this work is similar to that reported in ref. [19]. For dark matter whose mass is around 1 GHz, the expected signal window of the big flow axion dark matter is about 0.625 Hz [27] as mentioned earlier, corresponding to 25 frequency intervals with a $\Delta f = 0.025$ Hz. By 25 coadding such frequency points, one can search for the big flow axion dark matter. Other axion dark matter models with wider signal windows can be done as well with relevant data processing. The choice of an intermediate frequency (IF) of 1 MHz avoids the ϵ_{DAQ} decreasing too much and also maintains a manageable data size, which is to be discussed in section 3.

	ref. [19]	this work
frequency resolution bandwidth Δf	10 Hz	0.025 Hz
intermediate frequency (IF)	10.7 MHz	1 MHz
number of power spectra	5120	13
individual spectrum span	150 kHz	150 kHz
frequency tuning steps	10 kHz	10 kHz

Table 1. Parameters used in ref. [19] and this work. The numbers 5120 and 13 are numbers of power spectra taken for each resonance frequency step, where the former is in fact 40 power spectra with each being the average of 128 individual spectra [37].

3 DAQ efficiency

We used the same DAQ framework developed in our previous work [37], but used a different fast digitizer, M4i-4480-x8 from Spectrum Instrumentation GmbH [38]. The details of the DAQ realization are identical to those found in ref. [37]. The new fast digitizer also has two parallel channels and the main specifications of the analogue-to-digital converters (ADCs) are a 14-bit amplitude and a maximum sampling rate of 400 MSamples/s. The relevant parameters for this work are listed in table 2. The fast digitizer M4i-4470-x8 with a 16-bit amplitude and a maximum sampling rate of 180 MSamples/s from Spectrum Instrumentation GmbH [38] was used for refs. [19, 35, 37]. Therefore, the 45 MSamples/s

	ref. [19]	this work
sampling rate (MSamples/s)	45	3.125
ADC data points per individual power spectrum	4.5M	125M

Table 2. Parameters for the DAQ process used in ref. [19] and this work.

was chosen from $(180 \text{ MSamples/s})/2^2$ and 3.125 MSamples/s from $(400 \text{ MSamples/s})/2^7$. Figure 1 (a) shows a typical power spectrum from the fast digitizer applying the parameters in table 2 and the $50\text{-}\Omega$ terminations on the input ports as the noise sources. As expected,

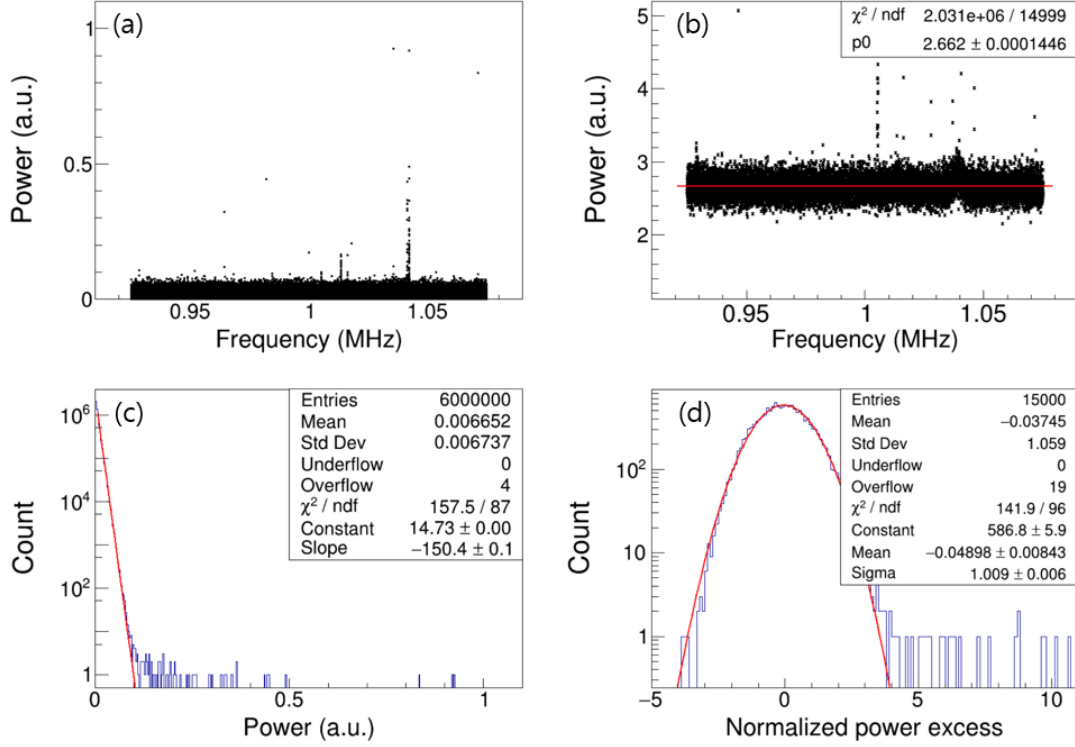


Figure 1. (a) shows a power spectrum in arbitrary units (a.u.) and $\Delta f = 0.025$ Hz obtained from the digitizer, where typical narrow peaks are also detected on top of the random noise. (b) results from (a) by merging 400 frequency points, and thus Δf becomes 10 Hz. (c) shows the power distribution from (a) and (d) the normalized power excess from (b) after background subtraction. The red lines in (b), (c), and (d) are a constant, an exponential, and a gaussian fit, respectively.

the noise power distribution shown in figure 1 (c) is almost exponential. Merging 400 frequency points in figure 1 (a) results in figure 1 (b) whose Δf becomes 10 Hz and the normalized power excess shown in figure 1 (d) follows a gaussian distribution as expected. The data size of the individual power spectra is about 210 MB to achieve $\Delta f = 0.025$ Hz, which is ~ 2.7 GB for each resonance frequency tuning step taking 13 power spectra, and ~ 5.5 TB for ~ 2000 resonance frequency tuning steps [19]. Retaining the IF of 10.7 MHz requires a sampling rate of at least 25 MSamples/s provided by the digitizer adopted in this work to satisfy the Nyquist rate [39], hence resulting a data size that is at least 8 times larger.

Our sampling rate of 3.125 MSamples/s introduces the signal aliasing from frequencies higher than about 1.56 MHz according to the Nyquist rate [39] and this can be avoided using a commercial low pass filter, e.g., LPF-B0R8+ [40]. The filter works well up to 1.1 MHz which is low enough to prevent the signal aliasing from frequencies above ~ 1.56 MHz. The frequency down conversion to IF also introduces unwanted image backgrounds which can be removed with an image rejection mixer. The working IF range for the image rejection mixer IRM0622B [41] used in refs. [19, 35] is 10 \sim 50 MHz which does not fit to the IF of 1 MHz for this work. The IQ (in-phase and quadrature) mixer QD0622B [41] is known to

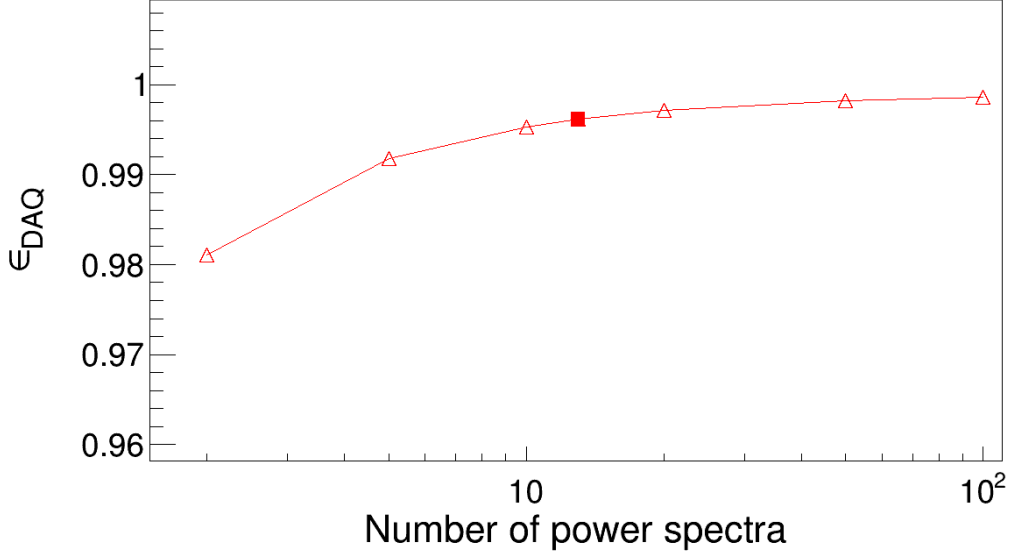


Figure 2. ϵ_{DAQ} as a function of the number of power spectra. The case where 13 power spectra are taken is denoted by the solid rectangle.

work for an IF value down to 100 kHz without introducing the potential IQ imbalance, and the image backgrounds can be removed with a proper signal processing combining I and Q signals from the IQ mixer.² Therefore, the two parallel channels on the fast digitizer have to be employed for the processing of the I and Q signals from the IQ mixer. The ϵ_{DAQ} was then estimated in the same way used in ref. [37] only when the IQ mixer and the two parallel channels were used, but the error estimation was done differently. Since our ϵ_{DAQ} does not follow the binomial statistics,³ the ϵ_{DAQ} error was estimated by checking the DAQ processing time for every individual power spectra. The deviation was at an order of 0.01% which is also consistent with the variance associated with 250M ADC data points per individual power spectrum. Therefore, such small error bars were not shown (were ignored) in figure 2. The data acquisition time is 40 s with $\Delta f = 0.025$ Hz and the online FFT time for 250M ADC data points from the two parallel channels is about 25 s. Hence, an extra 15 s is available and can be allocated for the digitizer-to-memory transfer of the ADC data and writing the FFT output to disk without any loss to the ϵ_{DAQ} [37].⁴ Because the next DAQ for the next resonance frequency step can simultaneously start with the last FFT in the current DAQ process, the time for the last FFT does not contribute to the ϵ_{DAQ} [37]. For taking 13 power spectra, the ϵ_{DAQ} is, therefore, over 99% and marked as the solid rectangle in figure 2. Even for a higher IF, the data acquisition time is 40 s for $\Delta f = 0.025$ Hz. However, if we were to take data for the higher resolution of $\Delta f = 0.025$ Hz for an IF of 10.7 MHz, online FFTs for 2G ADC data points provided by a sampling rate

²Note the IQ mixer and low pass filter were not directly used in this work and they are suggestions to figure out the addressed problems raised from the choice of such a low sampling rate.

³We used binomial statistics in our previous study [37] which led to the overestimated ϵ_{DAQ} errors.

⁴The ADC data was not saved to disk.

of 25 MSamples/s will need about 200 s. The expected ϵ_{DAQ} for this case is at most 20% even ignoring the ADC and FFT data transfers. Such a low ϵ_{DAQ} is hardly accepted in general, and thus lowering the IF from 10.7 MHz to 1 MHz is unavoidable.

4 Axion dark matter searches

Unlike figure 1 (b), the background shape in typical axion dark matter searches is not necessary flat, and looks like figure 3 (c) due to complicated properties of the cavity and the receiver chain. One sample of the data for axion dark matter searches in this work is

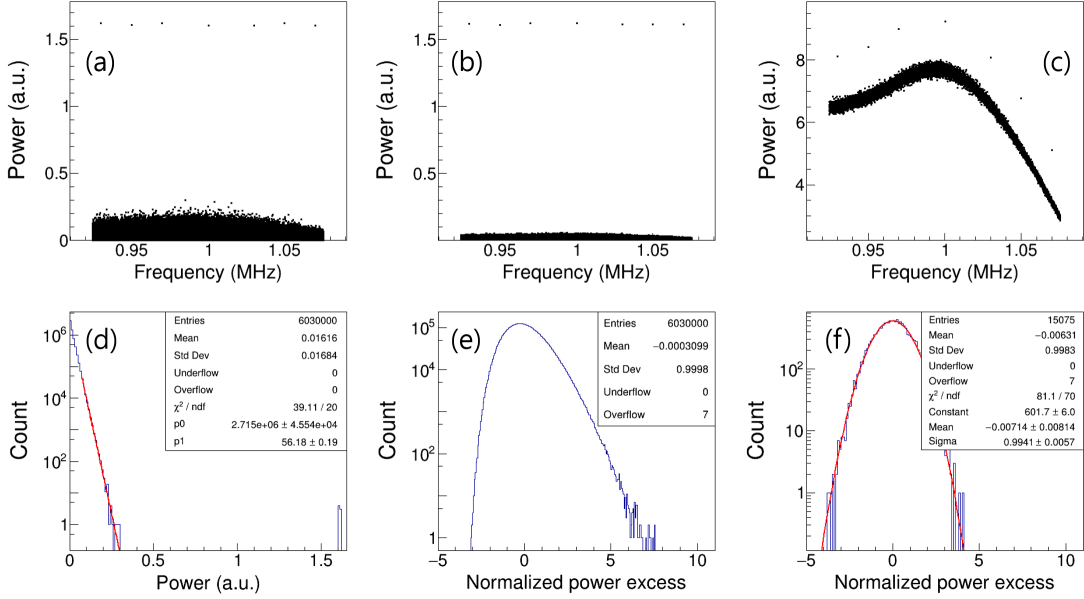


Figure 3. Simulation data when the axion mass matches the frequency of the cavity mode. (a) shows a simulated power spectrum with $\Delta f = 0.025$ Hz, where 7 narrow peaks are also added and the 4th narrow peak is located at the signal region. (b) is an averaged power spectrum over 13 power spectra, where one of them is shown in (a). (c) results from (b) by merging 400 frequency points, thus Δf becomes 10 Hz. (d) shows the power distribution from (a). (e) and (f) are the normalized power excess from (b) and (c) after background subtraction by a perfect fit, respectively. Note the 7 narrow peaks belong to the overflows in (e) and (f). The red lines in (d) and (f) are an exponential and a gaussian fit, respectively.

shown in figure 3, which is the case when the axion mass matches the resonance frequency of the cavity. Power at each frequency point whose frequency interval is 0.025 Hz shown in figure 3 (a) was generated following a χ^2 distribution with $2N_f$ degrees of freedom, where N_f is the number of frequency points [32]. As shown in figure 3 (a), (b), and (c), 7 narrow peaks are embedded to check the effect of the HR-RBW-filtering to the SNR efficiency ϵ_{SNR} . The 7 peaks are located over the whole spectrum including the signal region around the 4th peak. One can add more such peaks, but the current number of peaks is sufficient to represent the effects not only of the aforementioned filtering but also of the cavity response for unwanted spurious signals while the cavity is tuned to different

frequency tuning steps. The latter is seen in figure 6 (b) later. The HR-RBW-filtering condition for the data shown in figure 3 removes frequency points with power levels higher than 0.35. This value is obtained by identifying the outliers of an exponential fit shown in figure 3 (d), and is obvious through simple observation. Only the 7 unwanted narrow peaks are filtered out and the data is treated like stationary Poisson noise. Since this filtering was applied to all the individual power spectra whose RBW is 0.025 Hz, in this work it affects not only the big flow search using individual power spectra in figure 3 (a), but also the standard halo and tidal stream searches using that in figure 3 (c). The axion signal whose window size depends on the models, but with the same mass is added to the background. Thus, three data samples are used for the standard halo, the tidal stream, and the big flow, respectively. We also have another set without the 7 narrow peaks and refer to it as the “reference sample.” The ϵ_{SNR} due to background subtraction can be estimated analytically according to ref. [42] and is expected to be at most 93% using a suitable Savitzky-Golay filter [43]. Typical χ^2 parameterizations for background subtraction also provided about the same efficiency, where the efficiency was estimated from a large sample of simulation data [19]. Because the background subtraction efficiency is not the interest of this work, we used the simulation input background functions, i.e., a perfect fit, for background subtraction. Therefore, applying a perfect fit to the reference sample without any filtering of individual power spectra results in the SNR with an $\epsilon_{\text{SNR}} = 100\%$, where one filtering is the aforementioned HR-RBW-filtering for the big flow searches [31–34] and the other [44] for the standard halo and tidal stream axion dark matter searches. The latter filtering is referred to as the “LR-RBW-filtering” with an RBW of 10 Hz in this work, where LR stands for low resolution. The typical condition of the LR-RBW-filtering is for normalized power excess points that are larger than 4.5. This also removes the 7 narrow peaks corresponding to the 7 overflows shown in figure 3 (f).

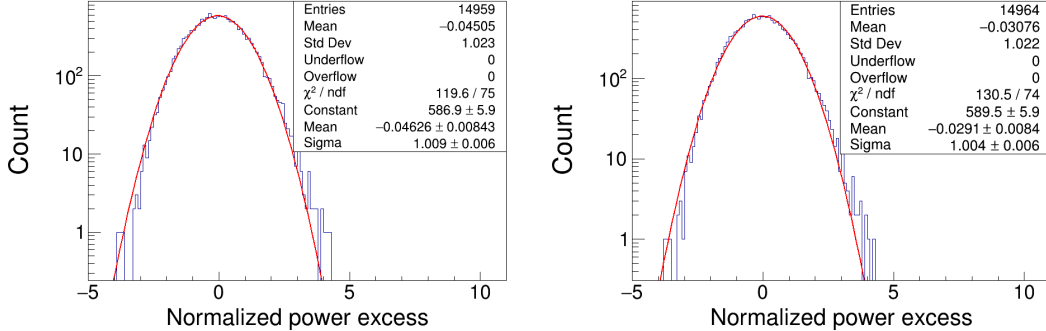


Figure 4. Normalized power excess distributions after applying the LR-RBW-filtering only (left) and both the HR-RBW-filtering and LR-RBW-filtering (right) to data shown in figure 1, respectively.

We applied the filtering to available data shown in figure 1. The HR-RBW-filtering condition for the data shown in figure 1 removes frequency points with power levels higher than 0.1 from the exponential fit shown in figure 1 (c). A constant fit shown in figure 1 (b) was used for the LR-RBW-filtering. Figure 4 shows the normalized power excess

distributions after applying the LR-RBW-filtering only (left) and the two-staged filtering (right), respectively. Since the latter figure has more data points (entries), it has filtered out less data and thus it is more efficient. Here, the difference is not that significant in the absence of the axion signal and when no further analysis processing is done, while we are able to demonstrate the effect is significant in the presence of the signal and with the full analysis procedure in the following sections.

4.1 Standard halo

The signal window of the standard halo axion dark matter is about 4 kHz for an axion frequency of about 1 GHz as in refs. [19, 20]. The standard halo axion dark matter signal

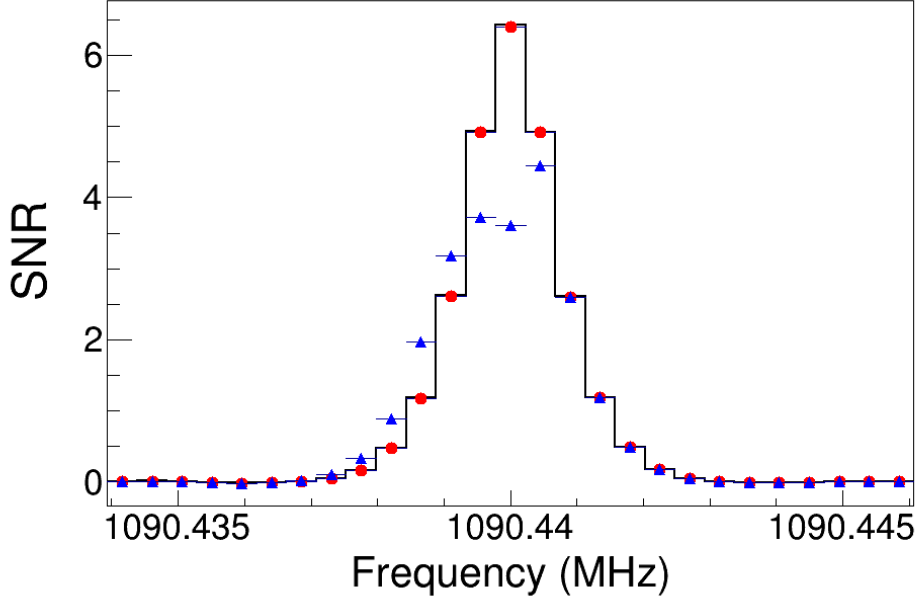


Figure 5. SNRs as a function of frequency around the signal region from 10000 simulated experiments. The black line is the case with an ϵ_{SNR} of 100%. The red circles are with applying both the HR-RBW-filtering and the LR-RBW-filtering and the blue triangles with the LR-RBW-filtering only.

was reconstructed following not only the procedure in ref. [19] which includes the LR-RBW-filtering, but also the additional HR-RBW-filtering. Hence the procedure steps in sequence, in view of figure 3, are the HR-RBW-filtering to the individual power spectra whose RBW is 0.025 Hz (figure 3 (a)), averaging over the 13 power spectra (figure 3 (b)), merging 400 frequency points resulting in an RBW of 10 Hz (figure 3 (c)), and finally background subtraction (figure 3 (f)). The LR-RBW-filtering was applied to the data shown in figure 3 (f). After the relevant overlapping and coadding steps, the SNRs as a function of frequency around the signal region from 10000 simulated experiments are shown in figure 5. The red circles and blue triangles in figure 5 are from data with the aforementioned narrow peak in the signal region, where the former was gone through the HR-RBW-filtering and LR-RBW-filtering and the latter the LR-RBW-filtering only. The

black line in figure 5 is from data without the narrow peak and its efficiency is 100% since it does not have any filtering. As shown in figure 5, the black line and red circles are almost identical, which means the HR-RBW-filtering efficiency is almost 100%. The SNR represented by the blue triangles, however, are significantly degraded at the signal frequency compared to that by the red circles, because the LR-RBW-filtering was triggered for narrow peaks in the blue triangle data, but not to the red circle data which has already removed such peaks with the HR-RBW-filtering. Such an SNR degradation is attributed by the LR-RBW-filtering condition, because the filtering usually removes the neighboring points as well as the narrow peak. The blue triangles resulted from removing ± 5 data points with respect to the peak position as done in ref. [19]. There exist subtle differences

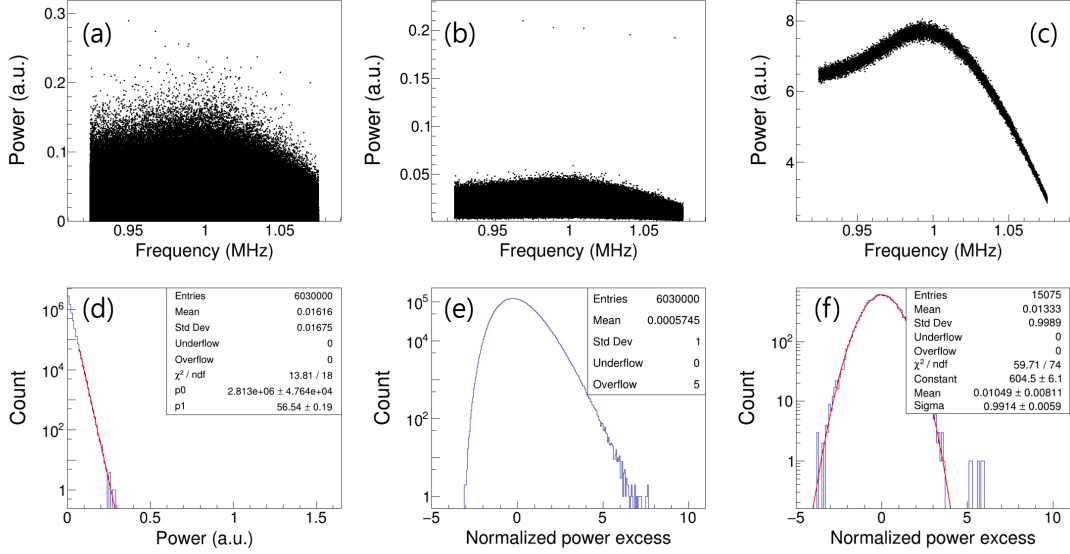


Figure 6. The same as figure 3 except for the frequency of the cavity mode, where it is 40 kHz away from the axion mass. Hence the axion signal is positioned at frequencies around the 4th narrow peak clearly shown in (b). The 5 overflows in (e) correspond to the 5 excesses whose SNRs are larger than 5 in (f).

between the black line and the red circles in figure 5 due to the narrow peak in the signal region when the frequency of the cavity mode sits away from the axion mass as shown in figure 6 (b). The data shown in figure 6 is the same as figure 3 except for the frequency of the cavity mode, where it is 40 kHz away from the axion mass. Due to the cavity response profiles, the amplitude of all the narrow peaks are suppressed down to below 0.35 as shown in figure 6 (a) and (d), which caused the HR-RBW-filtering to overlook these points. The LR-RBW-filtering was applied to the signal region for this data which still retains the spurious peaks as seen in figure 6 (f), but the amplitude of the signal power was also suppressed by the cavity response profiles, which resulted in the negligible filtering effect to the SNR as shown in red circles in figure 5. This subtle effect is more visible in the tidal stream axion dark matter search in section 4.2. For tuning steps where the cavity mode's resonance frequency sits farther away from the axion mass, the spurious narrow

peak will not be as much above the noise and can be overlooked by both the HR-RBW-filtering and LR-RBW-filtering. Only the surviving spurious peaks in the signal region from each frequency tuning step participate in the overlapping process. Depending on the filtering conditions, the peaks' contribution to the SNR during overlapping can vary. For LR-RBW-filtering, most of the data at the signal frequency is removed alongside the spurious peak when the cavity resonance is closer to the signal frequency. On the other hand, HR-RBW-filtering can do “pinpoint removals” of spurious peaks without affecting the rest of the data at high resolution. Thus, the contribution of surviving spurious peaks is higher for the blue triangles before coadding, due to the absence of the data when the cavity resonances are close to the axion mass. This leads to a higher-than-usual power excess at the signal frequency, at the cost of retained data at that point. The combined effects result in the SNR being skewed to the left, with some points showing better SNRs compared to the black line, after coadding with an asymmetric, boosted Maxwellian axion signal shape. In contrast, the red circles have relatively more data coming from the axion signal, and the surviving spurious peaks do not have such a pronounced effect on the SNR. As a result, the final coadded SNR closely follows the black line.

The SNR of about 6 by the red circle in figure 5 would be close to 5 after considering the aforementioned background subtraction efficiency and additional systematic effects, e.g., noise calibrations. Hence applying a typical threshold of 3.718 of the normalized power excess, one can get a one-sided 90% upper limit corresponding to an SNR of 5. Since the parameters used are similar to those in ref. [19], the sensitivity from the data generated in this work would be similar to that achieved in ref. [19], i.e., DFSZ sensitivity at a 90% CL.

4.2 Tidal stream

The tidal stream axion dark matter from the Sagittarius dwarf galaxy [25, 26] would have a signal window of about 150 Hz for an axion frequency of about 1 GHz as in ref. [35]. Even with such a narrow signal window, the averaging and overlapping of power spectra can be applied to the experiment [19, 20] to increase the SNR, according to ref. [35]. Hence the analysis procedure is basically the same as that for the standard halo axion dark matter search in the previous section 4.1. Due to the absence of a dedicated rescan schedule in ref. [35], a tighter LR-RBW-filtering, i.e., the removal of normalized power excesses higher than 3.5, was applied. The neighboring ± 1 data points with respect to the peak position were also removed. We can in general relieve the condition to 4.5 from 3.5 assuming a rescan. Allowing the averaging and overlapping and after the relevant coadding procedure, the SNRs as a function of frequency around the signal region from 10000 simulated experiments are shown in the left plot of figure 7. The green rectangles in left plot of figure 7 were obtained with the same LR-RBW-filtering condition in ref. [35] and the SNR at the signal frequency is about 91% with respect to that of the red circles in the same plot, which is consistent with the LR-RBW-filtering efficiency in ref. [35]. The red circles were obtained with the loose LR-RBW-filtering assuming the rescan. The SNR can be further improved from a coadding procedure with higher resolution RBW as seen in ref. [19]. The left and right plots of figure 7 result from 5 coadded frequency points with 30 Hz intervals and 15 coadded frequency points with 10 Hz intervals, respectively.

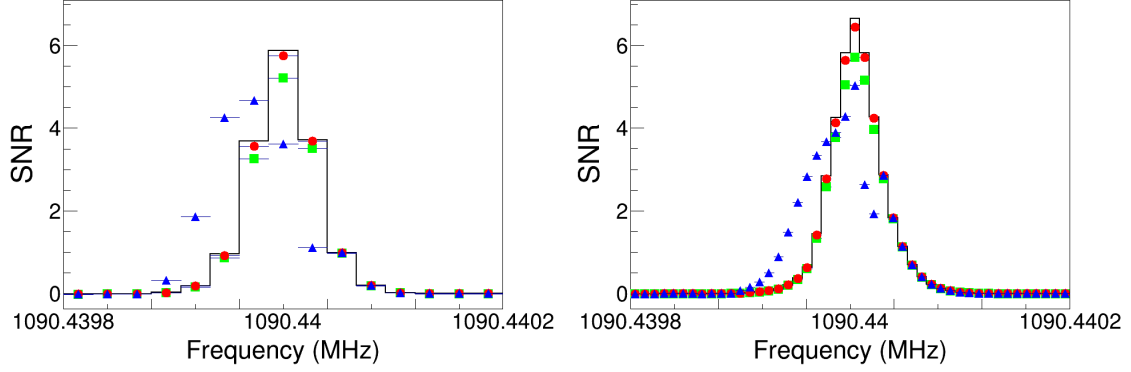


Figure 7. SNRs as a function of frequency around the signal region from 10000 simulated experiments. The black line is the case with an ϵ_{SNR} of 100%. The red circles are with applying both the HR-RBW-filtering and the LR-RBW-filtering and the blue triangles with the LR-RBW-filtering only, where the LR-RBW-filtering condition is the looser one, i.e., the normalized power exceeds greater than 4.5. The green rectangles are with applying both filtering but with the tighter LR-RBW-filtering with the normalized power exceeds greater than 3.5. Left followed the RBW reduction in ref. [35], i.e., 10 Hz to 30 Hz, then applied the coadding of 5 frequency points to ensure the signal window of 150 Hz, while right maintains the RBW of 10 Hz, then applied the coadding of 15 frequency points.

This ensures that both cases cover the signal window of 150 Hz. The SNRs in figure 7 were achieved with DFSZ axion dark matter that constitutes about 19.2% of the local dark matter density and the SNR by the red circle at the signal frequency in right plot is similar to the SNR of the standard halo axion dark matter search assuming $\rho_a = 0.45 \text{ GeV/cm}^3$. Therefore, a DAQ sensitive to the standard halo DFSZ axion dark matter that makes up 100% of the local dark matter density can also search for tidal stream DFSZ axion dark matter that constitutes about 19.2% of the local dark matter density simultaneously. Without HR-RBW-filtering, the SNRs by the blue triangles in figure 7 are worse at the signal frequency due to the same reason discussed in section 4.1.

The aforementioned discrepancy in the SNR of the black line and the red circles being more noticeable here than compared to figure 5 (for the standard halo axion dark matter search) is due to different LR-RBW-filtering conditions in this work. The tidal stream filter removes 30 Hz width of frequency points creating a larger effect on the 150 Hz signal window, compared to the standard halo, where the filter removes 110 Hz for a model whose signal window is 4050 Hz.

4.3 Big flow

The signal width of the big flow axion dark matter whose mass is about 1 GHz is expected to be less than 1 Hz. For such an extremely narrow signal window, the averaging and overlapping of power spectra are not applicable due to the signal frequency shift resulting from the rotational and orbital motions of Earth [35]. Therefore, only one power spectrum out of 13 power spectra collected in a frequency step was used for the big flow axion dark matter search. In order to benefit from the cavity resonance profiles and avoid the

overlapping of the power spectra, we only took a ± 5 kHz window with respect to the IF in individual power spectra for a given frequency tuning step of 10 kHz. Then, all the power spectra from each resonance frequency were combined without the averaging and overlapping to build the grand power spectrum. After coadding 25 frequency points to ensure a signal window of 0.625 Hz, figure 8 shows the normalized power excess distribution from the background only data (left) and the SNRs as a function of frequency around the signal region from 10000 simulated experiments (right). As shown in the left plot of figure 8,

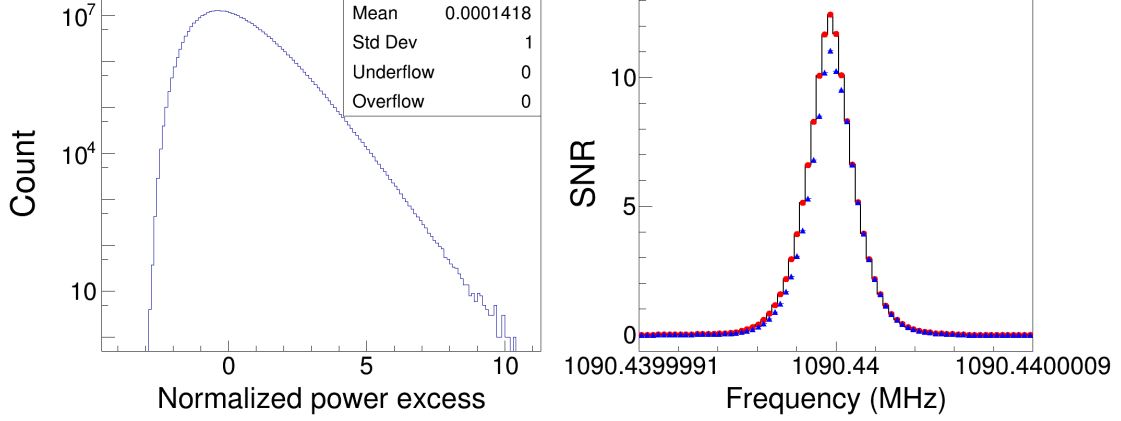


Figure 8. The normalized power excess distribution from the background only data after coadding 25 frequency points (left) and the SNRs as a function of frequency around the signal region from 10000 simulated experiments (right). The black line in the right plot is the case with an $\epsilon_{\text{SNR}} = 100\%$. The blue triangles and red circles are from data with and without the narrow peak background in the signal region, respectively, where they are with the HR-RBW-filtering.

the background in this case follows a non-gaussian distribution. From this distribution, we can get a one-sided 90% upper limit corresponding to an SNR of 10 by a threshold of 8.827 of the normalized power excess. Considering the inefficiencies and systematic effects, an SNR of about 12 marked as the red circle in the right plot of figure 8 would conservatively approach 10. The blue triangles in the right plot of figure 8 are from data with the narrow peaking background in the signal region, thus showing unavoidable SNR degradation compared to the red circles from data without the peaking.

The SNR of the red circle at the signal frequency in the right plot of figure 8 was achieved with DFSZ axion dark matter that constitutes about 12.4% of the local dark matter density. Therefore, big flows with these characteristics can be searched for using the same DAQ that is sensitive to standard halo DFSZ axion dark matter that constitutes 100% of the local dark matter density $\rho_a = 0.45 \text{ GeV/cm}^3$.

5 Summary

We show axion dark matter searches covering the standard halo, the tidal stream, and the big flow employing a DAQ channel with a single HR RBW, without sacrificing the ϵ_{DAQ} , where the DAQ process includes online FFTs and writing the outputs to disk. Assuming

that the total amount of data from DAQ is sensitive to the standard halo DFSZ axion dark matter whose $\rho_a = 0.45 \text{ GeV/cm}^3$, then the same data also provides the tidal stream and the big flow axion dark matter searches that would be sensitive to DFSZ axion dark matter that constitute 19.2% and 12.4% of the local dark matter densities, respectively, at a 90% CL. We also report that the filtering of the individual power spectra acquired with an HR RBW, e.g., for the big flow search can prevent a possible significant degradation in the SNR from the searches in the lower resolution RBW's, i.e., the standard halo and tidal stream searches. The difference in the degradation of SNR is quantified in table 3. Table 3 provides the expected SNRs assuming DFSZ axions make up 100% of the local dark matter density and shows the novelty of this work relative to refs. [19, 35]. The HR RBW data acquisition allows for big flow searches to be possible and better SNR using two-staged filtering in SHM and tidal searches compared to previous analyses.

	[19, 35] with the LR-RBW-filtering only	this work with the two-staged filtering
SHM	4.4	6.4
tidal stream	4.7	5.7

Table 3. Expected SNRs assuming DFSZ axions with $\rho_a = 0.45 \text{ GeV/cm}^3$, when a narrow spurious peak is located at the signal region. The numbers with the two-staged filtering were chosen at the axion mass, while those with LR-RBW-filtering only as the maximum value around the axion mass in their skewed SNR distributions shown in figures 5 and 7.

Acknowledgments

This work was supported by a Korea University Grant, the National Research Foundation of Korea (NRF) grants funded by the Korea government (MSIT) (RS-2025-00556247) and (RS-2022-00143178), and the Korea Basic Science Institute (National research Facilities and Equipment Center) grant funded by the Korea government (MSIT) (NFEC-2019R1A6C1010027).

References

- [1] P. A. R. Ade *et al.* (Planck Collaboration), *Astron. Astrophys.* **594** (2016) A13.
- [2] V. Rubin and W. K. Ford Jr., *ApJ* **159** (1970) 379.
- [3] Douglas Clowe *et al.*, *ApJ* **648** (2006) L109.
- [4] S. Weinberg, *Phys. Rev. Lett.* **40** (1978) 223.
- [5] F. Wilczek, *Phys. Rev. Lett.* **40** (1978) 279.
- [6] G. 't Hooft, *Phys. Rev. Lett.* **37** (1976) 8.
- [7] G. 't Hooft, *Phys. Rev. D* **14** (1976) 3432; **18** (1978) 2199(E).
- [8] J. H. Smith, E. M. Purcell, and N. F. Ramsey, *Phys. Rev.* **108** (1957) 120.

- [9] W. B. Dress, P. D. Miller, J. M. Pendlebury, P. Perrin, and N. F. Ramsey, Phys. Rev. D **15** (1977) 9.
- [10] I. S. Altarev *et al.*, Nucl. Phys. **A341** (1980) 269.
- [11] R. D. Peccei and H. R. Quinn, Phys. Rev. Lett. **38** (1977) 1440.
- [12] P. Sikivie, Phys. Rev. Lett. **51** (1983) 1415.
- [13] P. Sikivie, Phys. Rev. D **32** (1985) 2988.
- [14] A. R. Zhitnitskii, Yad. Fiz. **31** (1980) 497 [Sov. J. Nucl. Phys. **31** (1980) 260].
- [15] M. Dine, W. Fischler, and M. Srednicki, Phys. Lett. **104B** (1981) 199.
- [16] N. Du *et al.* (ADMX Collaboration), Phys. Rev. Lett. **120** (2018) 151301.
- [17] T. Braine *et al.* (ADMX Collaboration), Phys. Rev. Lett. **124** (2020) 101303.
- [18] C. Bartram *et al.* (ADMX Collaboration), Phys. Rev. Lett. **127** (2021) 261803.
- [19] Andrew K. Yi *et al.*, Phys. Rev. Lett. **130** (2023) 071002.
- [20] Saebyeok Ahn *et al.*, Phys. Rev. X **14** (2024) 031023.
- [21] P. Salucci, F. Nesti, G. Gentile, and C. Frigerio Martins, A&A **523** (2010) A83.
- [22] Fabrizio Nesti and Paolo Salucci, JCAP **07** (2013) 016.
- [23] M. S. Turner, Phys. Rev. D **42** (1990) 3572.
- [24] Howard Georgi and S. L. Glashow, Phys. Rev. Lett. **32** (1974) 438.
- [25] K. Freese, P. Gondolo, H. J. Newberg, and M. Lewis, Phys. Rev. Lett. **92** (2004) 111301.
- [26] K. Freese, P. Gondolo, and H. J. Newberg, Phys. Rev. D **71** (2005) 043516.
- [27] P. Sikivie, Phys. Lett. B **567** (2003) 1.
- [28] Amina Helmi, Simon D. M. White, and Volker Springel, Phys. Rev. D **66** (2002) 063502.
- [29] Jürg Diemand and Michael Kuhlen, ApJ, **680** (2008) L25.
- [30] K. Dolag, A. D. Dolgov, and I. I. Tkachev, JETP Lett. **96** (2013) 754-758.
- [31] L. Duffy *et al.*, Phys. Rev. Lett. **95** (2005) 091304.
- [32] L. Duffy *et al.*, Phys. Rev. D **74** (2006) 012006.
- [33] J. Hoskins *et al.*, Phys. Rev. D **84** (2011) 121302(R).
- [34] J. Hoskins *et al.*, Phys. Rev. D **94** (2016) 082001.
- [35] Andrew K. Yi *et al.*, Phys. Rev. D **108** (2023) L021304.
- [36] Javier De Miguel, Abaz Kryemadhi, and Konstantin Zioutas, Phys. Rev. D **111** (2025) 023016.
- [37] S. Ahn *et al.*, JINST **17** (2022) P05025.
- [38] <https://spectrum-instrumentation.com>.
- [39] Harry Nyquist, Trans. AIEE, vol.47, pp. 617-644, Apr. 1928; Proc. IEEE, Vol. 90, No.2, Feb 2002.
- [40] <https://www.minicircuits.com>.
- [41] <https://polyphasemicrowave.com>.

- [42] A. K. Yi, S. Ahn, B. R. Ko, and Y. K. Semertzidis, J. High Energ. Phys. **11** (2023) 115.
- [43] A. Savitzky and M. J. E. Golay, Anal. Chem. **36** (1964) 1627.
- [44] B. M. Brubaker, L. Zhong, S. K. Lamoreaux, K. W. Lehnert, and K. A. van Bibber, Phys. Rev D **96** (2017) 123008.